Journal of Alloys and Compounds 866 (2021) 158904

Contents lists available at ScienceDirect

Journal of Alloys and Compounds

journal homepage: www.elsevier.com/locate/jalcom

Effect of Re and Ru on the phase stability and coarsening kinetics of $L1_2$ phase in a $Ni_{29}Co_{27}Fe_{27}Cr_3Al_7Ti_7$ high entropy alloy

Kaiwei Zhang [a], Feng He [a,b,*], Zhongsheng Yang [a], Dingcong Cui [a], Junjie Li [a], Zenan Yang [c], Jincheng Wang [a], Zhijun Wang [a,**]

[a] State Key Laboratory of Solidification Processing, Northwestern Polytechnical University, Xi'an 710072, PR China
[b] Centre for Advanced Nuclear Safety and Sustainable Development, City University of Hong Kong, Hong Kong, PR China
[c] Science and Technology on Advanced High Temperature Structural Materials Laboratory, Beijing Institute of Aeronautical Materials, Beijing 100095, PR China

ARTICLE INFO

Article history:
Received 7 December 2020
Received in revised form 22 January 2021
Accepted 23 January 2021
Available online 2 February 2021

Keywords:
High entropy alloy
Phase stability
Coarsening kinetics

ABSTRACT

The thermal stability of precipitates is a major concern for $L1_2$-type strengthening high entropy alloy at elevated temperatures. In this study, we systematically investigated the effect of Re and Ru on the phase stability an d coarsening kinetics of $L1_2$ precipitates in the $Ni_{29}Co_{27}Fe_{27}Cr_3Al_7Ti_7$ HEA. The $L1_2$ phase exhibited a high volume fraction of 40.29% in the explored HEA and remained a stable morphology during the long-term exposure. Re addition did not change the volume fraction of $L1_2$ phase, while Ru addition decreased it to 34.42%. Both Re and Ru facilitated the formation of $L2_1$ precipitates slightly. Minor Re significantly decreased the coarsening rate of $L1_2$ phase and minor Ru also retarded the coarsening of $L1_2$ phase to some degree, which were mainly ascribed to the sluggish diffusion of Re and Ru atoms. These findings provide a feasible strategy to improve the coarsening resistance of $L1_2$ precipitates in HEA system through sluggish atomic diffusion.

1. Introduction

Precipitation hardened high entropy alloys (HEAs), which combined the advantages of high-entropy matrix and precipitation hardening, have shown excellent strength-ductility combination [1–3]. Different precipitates, such as σ, μ, γ' and γ'' phases, have been used as effective strengthening phases in fcc-type HEAs [4–10]. For instance, Liu et al. [4]. used hard σ and μ precipitates to strengthen $CoCrFeNiMo_{0.3}$ HEA but the effect seemed to be limited. He et al. [5]. designed high-entropy γ'' phase, which showed superior strengthening effect. It was also reported that high-density $L1_2$ nanoparticles strengthened alloys achieved superb strengths of 1.5 Gpa and ductility as high as 50% in tension [6–8]. Among these precipitation-hardened HEAs, the $L1_2$-strengthened HEAs have shown great potential to be used as the next generation high-temperature materials [9,10]. At elevated temperatures, the thermal stability of the coherent precipitates is a main concern for high-temperature performance. Consequently, it is urgent to design $L1_2$ phase with good phase stability and coarsening resistance to keep excellent mechanical properties at high temperatures.

Recent efforts have demonstrated that the $L1_2$ precipitates in HEAs showed sluggish coarsening behaviors [11–15]. It was also widely reported that element diffusion in HEA was significantly slower than that in the case of conventional alloys [1,10]. Zhao et al. [11]. revealed that the coarsening rate of $L1_2$ phase in the $(NiCoCrFe)_{94}Al_4Ti_2$ HEA was much smaller than that of some superalloys and attributed this good coarsening resistance to the sluggish diffusion of Al or Ti in the high-entropy matrix. What is more, a remarkable sluggish coarsening behavior of $L1_2$ nanoparticles has been experimentally demonstrated in the $(NiCoCr)_{94}Al_3Ti_3$ MEA, in which Co atom was regarded as the origin that slowed down the coarsening process [12]. Peng et al. [13]. declared a small coarsening rate constant of $L1_2$ phase in $Ni_{28}Co_{28}Fe_{21}Cr_{15}Al_4Ti_4$ and He et al. [14]. reported that $L1_2$ phase in $Ni_2CoCrFeTi_xAl_y$ HEAs had remarkably slow coarsening rate at 800 °C as well. Yang et al. [15]. found that the activation energy of diffusion in Ni-30Co-13Fe-15Cr-6Al-6Ti-0.1B was significantly higher than that of conventional Ni- and Co-based superalloys, thus retarding the coarsening of $L1_2$ precipitates. All these studies indicated that the diffusion of component elements determined the coarsening resistance, and thus it is reasonable to speculate that addition of slowly diffusing elements could further improve the coarsening resistance of $L1_2$ nanoprecipitates in HEAs.

In the light of former literatures, Re was illustrated as the most effective element in improving high temperature capability in Ni-based

* Corresponding author at: State Key Laboratory of Solidification Processing, Northwestern Polytechnical University, Xi'an 710072, PR China.
** Corresponding author.
E-mail addresses: fenghe@mail.nwpu.edu.cn (F. He), zhjwang@nwpu.edu.cn (Z. Wang).

https://doi.org/10.1016/j.jallcom.2021.158904
0925-8388/

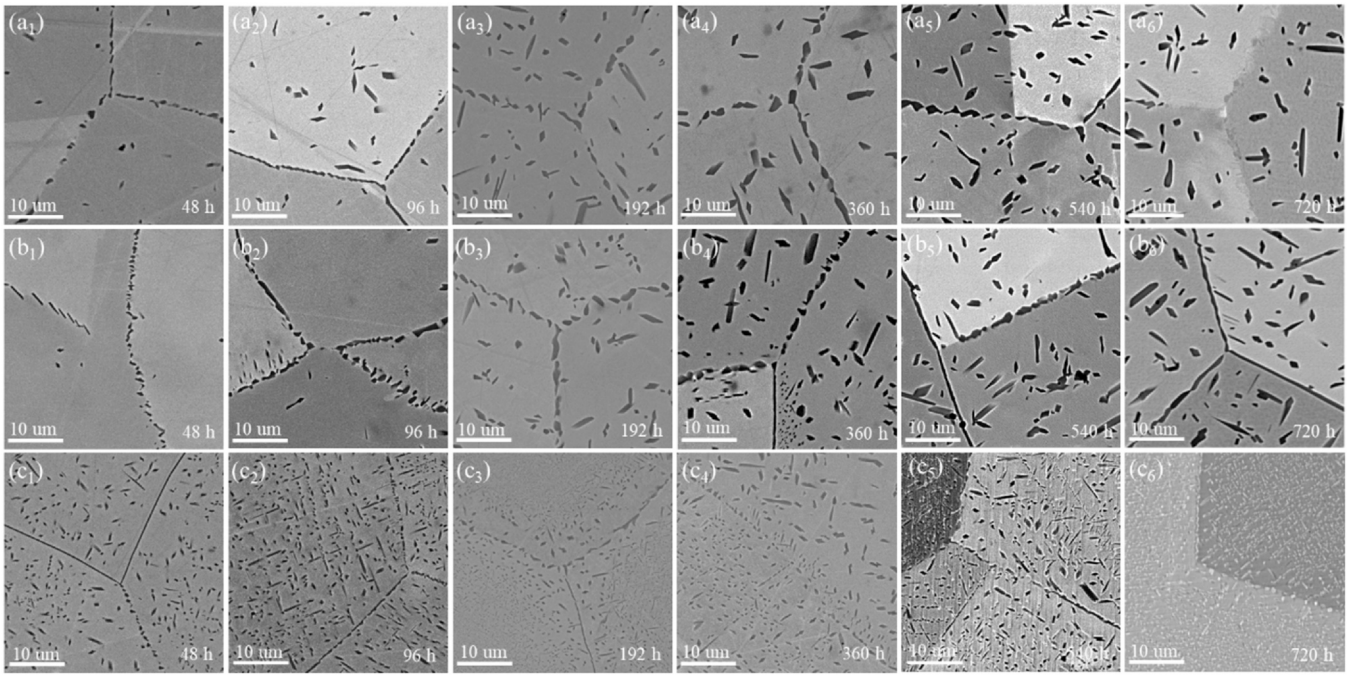

Fig. 1. SEM-BSE images of three HEAs aged at 800 ℃ for different time; (a) $Ni_{29}Co_{27}Fe_{27}Cr_3Al_7Ti_7$ HEA, (b) $Ni_{28}Co_{27}Fe_{27}Cr_3Al_7Ti_7Re_1$ HEA, (c) $Ni_{28}Co_{27}Fe_{27}Cr_3Al_7Ti_7Ru_1$ HEA.

superalloy [16]. Neumeier et al. [17]. demonstrated that Re was the slowest diffusing element in FCC Co among Re, W, Mo and Ta, using diffusion couples and first principles kinetic Monte Carlo. Recently, Zhang et al. [18]. found that Re constituted the rate-limited step for coarsening in a Re-containing Ni-based single crystal superalloy. Pandey et al. [19]. revealed that the slower coarsening rate of $L1_2$ phase in Co-30Ni-10Al-5Mo-2Nb-2Re superalloy was attributed to the slow diffusivity of Re in the FCC matrix and the Re-induced coagulation mechanism. Yoon et al. [20]. also reported that the addition of Re retarded the coarsening kinetics and stabilized the spheroidal morphology of $L1_2$ precipitates in Ni-Cr-Al superalloy. Ru as another alloying element has been introduced to manipulate the microstructure and property in some superalloys. According to previously published results, Ru additions reduced the tendency for formation of TCP phases, and dramatically improved the creep performance of Ni-based single-crystal superalloys [21,22]. It has also been reported that Ru had an effect on misfit and precipitate shape by influencing element partitioning in Ni-based superalloy [23]. Additionally, Sauza et al. [24]. demonstrated that the coarsening kinetics of $L1_2$ phase was decelerated to some degree by the addition of Ru to Co-Al-W superalloy. What is more, the diffusion coefficient of Ru is fairly small in Ni and Co [17,25]. It is consequently expected that the addition of Re and Ru would improve the coarsening resistance of $L1_2$ phase in HEAs. However, to our best knowledge, the effect of Re and Ru on the phase stability and coarsening kinetics of $L1_2$ phase in HEAs is less-explored.

In this study, we investigated the effect of Re and Ru on the phase stability and coarsening behavior of $L1_2$ precipitates in $Ni_{29}Co_{27}Fe_{27}Cr_3Al_7Ti_7$, which has shown excellent mechanical

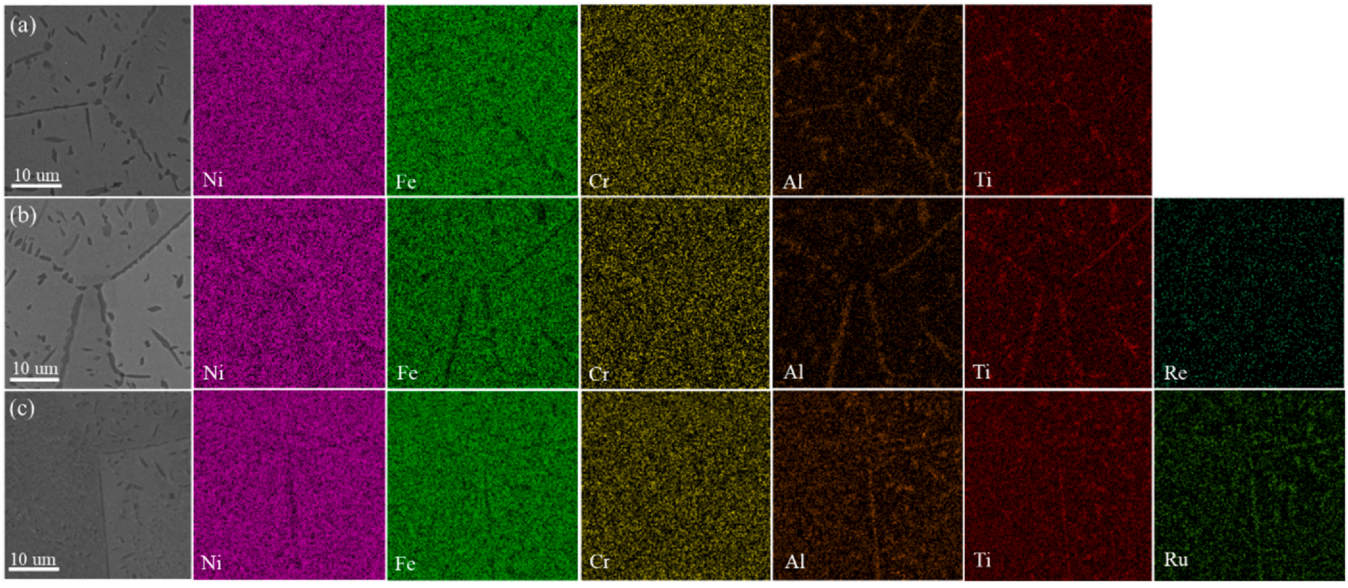

Fig. 2. EDS maps of three HEAs aged at 800 ℃ for 720 h; (a) $Ni_{29}Co_{27}Fe_{27}Cr_3Al_7Ti_7$ HEA, (b) $Ni_{28}Co_{27}Fe_{27}Cr_3Al_7Ti_7Re_1$ HEA, (c) $Ni_{28}Co_{27}Fe_{27}Cr_3Al_7Ti_7Ru_1$ HEA.

Table 1
EDS results showing the approximate element content of matrix and the blocky precipitates.

Atom fraction (%)		Ni	Co	Fe	Cr	Al	Ti	Re	Ru
AlTi	Matrix	31.4	26.4	26.5	3.1	5.3	7.3		
	$L2_1$	22.6	29.3	16.6	1.7	16.9	12.9		
AlTiRe	Matrix	29.2	27.5	27.9	3.2	5.1	6.8	0.3	
	$L2_1$	22.4	28.7	14.7	1.3	19.3	13.7	0.03	
AlTiRu	Matrix	30.9	26.4	27.8	3.1	4.8	6.5		0.4
	$L2_1$	21.7	27.1	17.6	2.0	16.8	12.2		2.5

properties [8,26]. With the aid of SEM, XRD, and EDS, we revealed that Ru promoted the formation of $L2_1$ phase and the Re significantly decreased the coarsening rate of $L1_2$ phase. The corresponding mechanisms were discussed based on LSW analysis and CALPHAD simulation.

2. Experimental procedure

The nominal $Ni_{29}Co_{27}Fe_{27}Cr_3Al_7Ti_7$ (at%) HEA, $Ni_{28}Co_{27}Fe_{27}Cr_3Al_7Ti_7Re_1$ (at%) HEA and $Ni_{28}Co_{27}Fe_{27}Cr_3Al_7Ti_7Ru_1$ (at%) HEA were prepared using arc melting and casted into a copper mold with the dimension of $50 \times 10 \times 5mm^3$. Elements of Ni, Co, Fe, Cr, Al, Ti, Re and Ru with high purity (> 99.92%) were used as raw materials. The ingots were flipped over and re-melted for at least four times to reduce the macroscopic inhomogeneity in composition and microstructure. The as-cast ingots were first solution-treated at 1200 ℃ for 2 h and then cold-rolled along the longitudinal direction with a total thickness reduction of ~70%, followed by recrystallization at 1200 ℃ for ~4 min. Subsequently, isothermal aging treatments were applied for the three HEAs at 800 ℃ for various durations from 1 h to 720 h. All the heat treatment procedures described here were finished by water quenching.

The SEM specimens were prepared by mechanically grinding, polishing in diamond suspension, and then polishing in colloidal silica suspension, analyzed by scanning electron microscope equipped with BSE and EDS detector (SEM, Tascan MIRA3). These samples were then used to conduct X-Ray diffraction (XRD) measurement using Rigakud/max-2550 equipped with monochrometer. ImageJ and photoshop CC 2019 softwares were used for image analysis. The average Vickers hardness was determined by adopting 10 testing points for each alloy sample, under a load of 1000 g with a dwell time of 15 s, using Micro Hardness Tester (Mode I: TH701). The phase diagrams were predicted by JmatPro 7.0 based on the database of nickel-based superalloy.

3. Results

3.1. Microstructures of the aged samples

Fig. 1 shows the backscattered electron images of three HEAs aged at 800 ℃ from 48 h to 720 h. In general, a similar precipitation

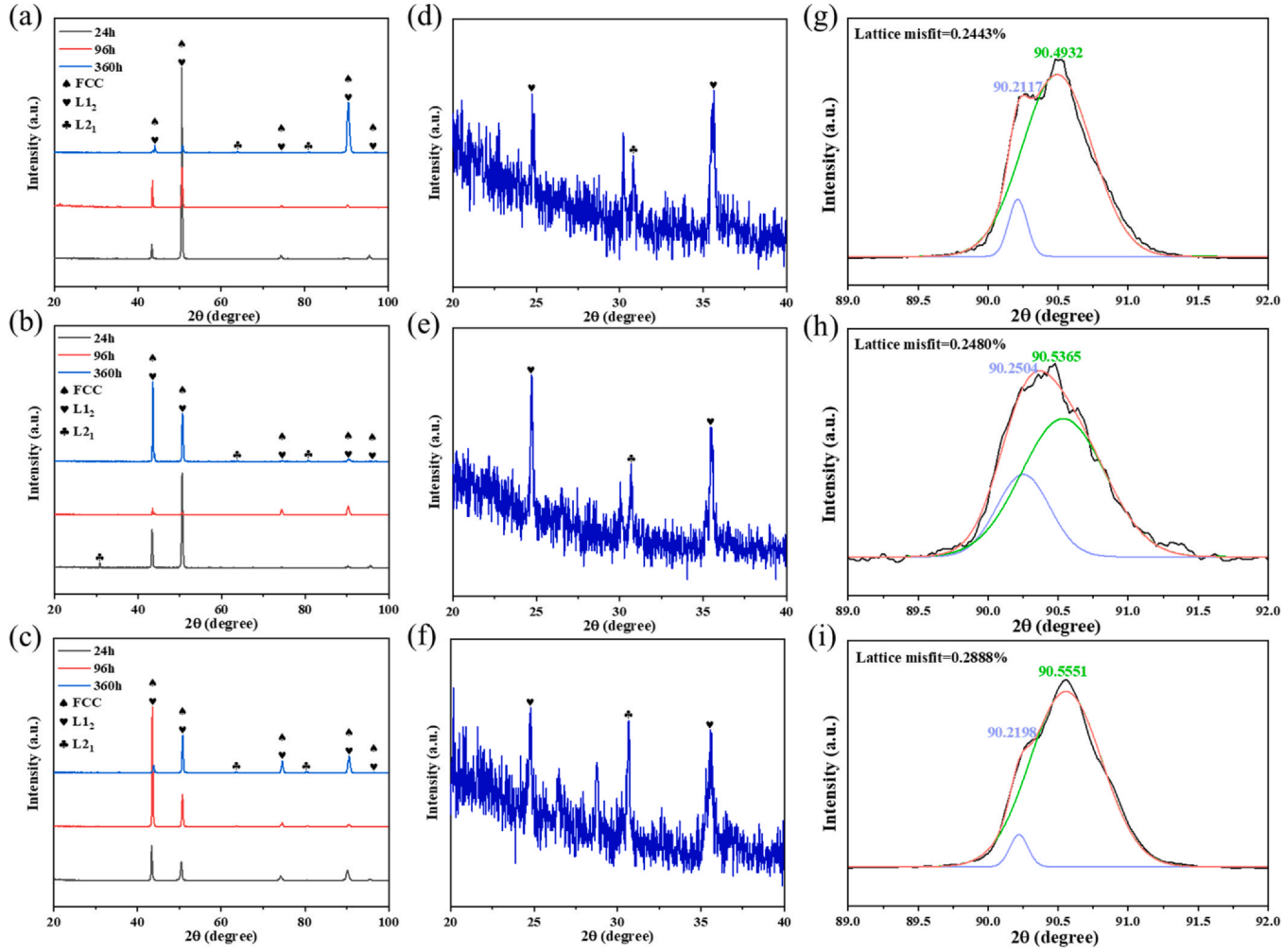

Fig. 3. XRD patterns showing the phase compositions of three HEAs aged at 800 ℃ for 24 h, 96 h and 360 h; (a) $Ni_{29}Co_{27}Fe_{27}Cr_3Al_7Ti_7$ HEA, (b) $Ni_{28}Co_{27}Fe_{27}Cr_3Al_7Ti_7Re_1$ HEA, (c) $Ni_{28}Co_{27}Fe_{27}Cr_3Al_7Ti_7Ru_1$ HEA. (d–f) Enlarged XRD patterns exhibiting small characteristic peaks of the three HEAs aged at 800 ℃ for 360 h. (g–i) Deconvolution of the (311) diffraction peaks of our three HEAs aged at 800 ℃ for 360 h, giving lattice misfit between $L1_2$ precipitate and FCC matrix.

Table 2
Lattice parameters of matrix and $L1_2$ phase, lattice misfits between these two phases (δ), volume fraction of $L1_2$ precipitate (φ), and coarsening constants of the $L1_2$ precipitate for our HEAs and other Ni-based alloys at 800 ℃.

HEAs	a_{L1_2}(nm)	a_{FCC} (nm)	φ_{L1_2}	|δ|	K(m^3/s)
$Ni_{29}Co_{27}Fe_{27}Cr_3Al_7Ti_7$	0.36063	0.35975	40.29%	0.2443%	1.48×10^{-27}
$Ni_{28}Co_{27}Fe_{27}Cr_3Al_7Ti_7Re_1$	0.36051	0.35961	39.97%	0.2480%	6.09×10^{-28}
$Ni_{28}Co_{27}Fe_{27}Cr_3Al_7Ti_7Ru_1$	0.36060	0.35956	34.42%	0.2888%	1.04×10^{-27}
Ni-21.7Co-13.4Al			23%		2.12×10^{-27}
Nimonic 105					2.67×10^{-27}
$Ni_{28}Co_{28}Fe_{21}Cr_{15}Al_4Ti_4$			29.83%		0.31×10^{-27}

behavior can be clearly identified for $Ni_{29}Co_{27}Fe_{27}Cr_3Al_7Ti_7$ (referred to as AlTi hereafter) and $Ni_{28}Co_{27}Fe_{27}Cr_3Al_7Ti_7Re_1$ (referred to as AlTiRe hereafter), but there was a significant difference in $Ni_{28}Co_{27}Fe_{27}Cr_3Al_7Ti_7Ru_1$ (referred to as AlTiRu hereafter) sample. For AlTi and AlTiRe alloy, blocky particles with micron sizes were observed at the grain boundaries (referred to as GBs hereafter) region, and only a few particles formed within grain interior in the early aging stage. The number and size of blocky particles in grain interior increased along with prolonged aging time. The particle sizes for AlTiRu HEA, by contrast, were smaller than those in AlTi and AlTiRe samples. As shown in Fig. 1c, however, the distribution of blocky particles in AlTiRu alloy was much more dispersive, compared with AlTi and AlTiRe samples.

SEM-EDS analyses were conducted to determine the element distribution of these blocky particles in HEAs aged at 800 ℃ for 720 h, as shown in Fig. 2. The corresponding EDS images showed that these large particles are enriched in Al, Ti and depleted in Ni, Fe, Cr among the three HEAs. Re partitioned to matrix in AlTiRe HEA (Fig. 2b), while Ru partitioned to these large precipitates in AlTiRu sample (Fig. 2c). EDS results in Table 1 show the approximate element content within matrix and blocky particles. It can be seen that the blocky precipitates contain more than 16 at% Al and 12 at% Ti, while lower than 23 at% Ni, 18 at% Fe and 2 at% Cr for three HEAs. Additionally, the large particles contain only about 0.03 at% Re for AlTiRe alloy, while it contains about 2.5 at% Ru in AlTiRu sample.

XRD patterns of three HEAs aged at 800 ℃ for different times are presented in Fig. 3, which show similar diffraction peaks among three HEAs. Besides the typical FCC-$L1_2$ dual-phase diffraction patterns, we also characterized the $L2_1$-phase (a highly ordered BCC structure). Figs. 3d–f exhibit small characteristic peaks of $L1_2$-phase and $L2_1$-phase of three HEAs aged at 800 ℃ for 360 h. After 360 h of isothermal heat treatment, other intermetallic phases were not observed. It is clear that the $L2_1$-phase represents for the blocky precipitates at GBs and within grain interiors, as mentioned earlier in SEM images. Furthermore, the lattice mismatch values between $L1_2$ precipitate and FCC matrix were calculated by XRD analysis from the (311) diffraction peaks. We determined the lattice mismatch of the $L1_2$-matrix of 0.2443% for the AlTi alloy, 0.2480% for the AlTiRe alloy and 0.2888% for the AlTiRu alloy (Fig. 3g–i and Table 2).

3.2. Ripening of $L1_2$ precipitates

Fig. 4a–c display the representative high-resolution BSE images of three HEAs isothermally aged at 800 ℃ for different time intervals. It was evident that the uniform $L1_2$ precipitates were embedded in the FCC matrix. The morphology of the $L1_2$ particles in the three HEAs remained cuboidal with rounded corner till heat-treated for

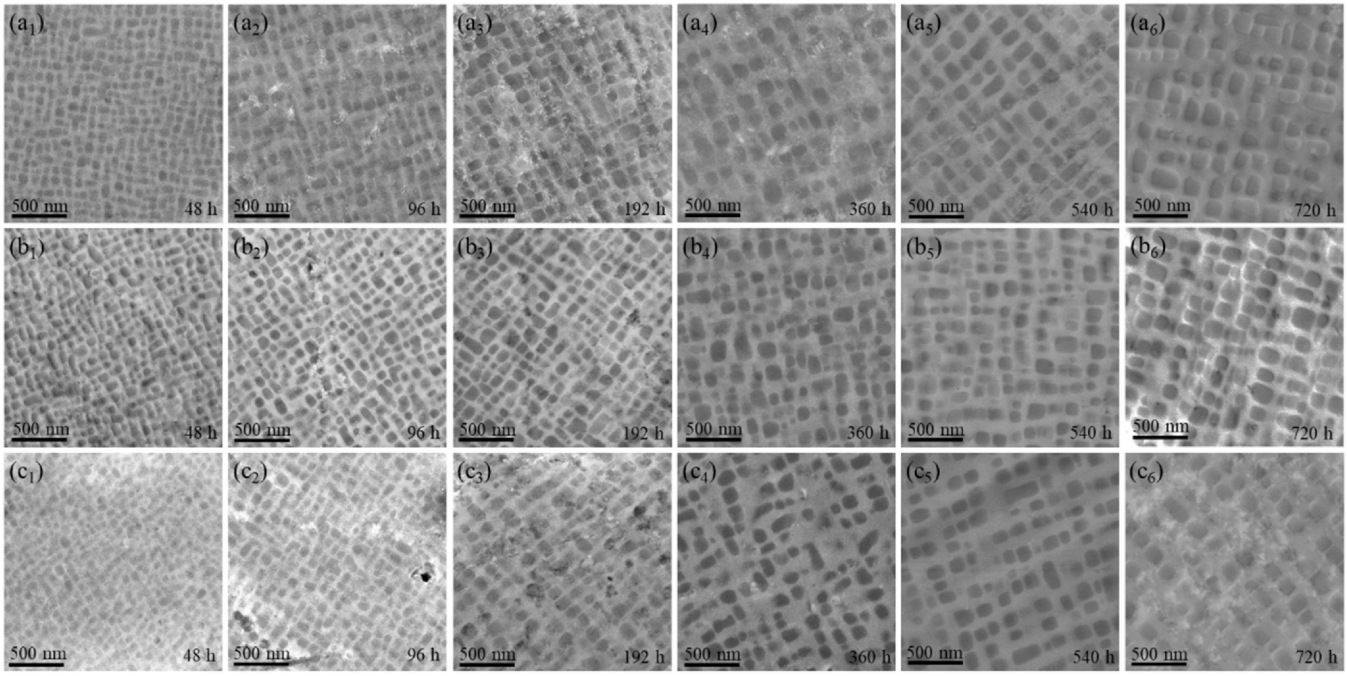

Fig. 4. SEM-BSE images of three HEAs aged at 800 ℃ for different time, revealing the evolution of high-density $L1_2$ precipitates within grain interior; (a) $Ni_{29}Co_{27}Fe_{27}Cr_3Al_7Ti_7$ HEA, (b) $Ni_{28}Co_{27}Fe_{27}Cr_3Al_7Ti_7Re_1$ HEA, (c) $Ni_{28}Co_{27}Fe_{27}Cr_3Al_7Ti_7Ru_1$ HEA.

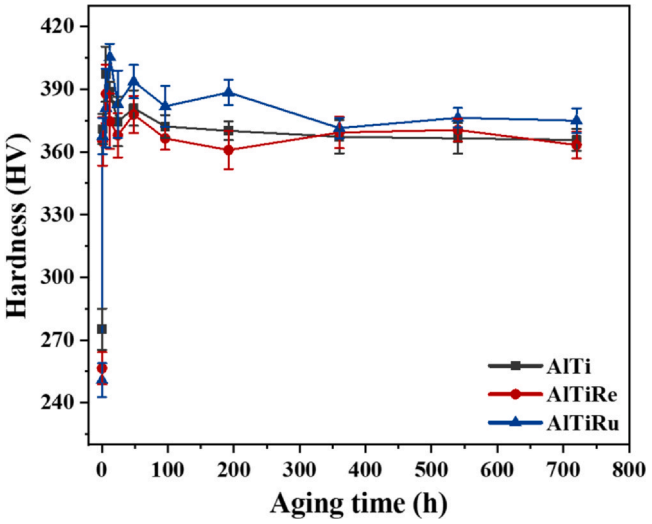

Fig. 5. Evolution of Vickers micro-hardness number (HV) for three HEAs during isothermal heat-treatment at 800 ℃.

720 h. Analogously, the particle size increased while the number density decreased with the aging time. The average diameter of $L1_2$ precipitates increased from 73.4 nm after aging for 48 h to 157.0 nm after aging for 720 h of AlTi HEA, from 67.9 nm to 122.5 nm for AlTiRe HEA, from 68.7 nm to 143.6 nm for AlTiRu HEA, respectively.

3.3. Hardness

The mechanical stability of three HEAs during long term exposure was evaluated by measuring room-temperature microhardness values of different aging time, which are plotted in Fig. 5. It could be noted that a dramatic rise in the hardness value was observed in the early aging stage among three HEAs. Compared to the merely recrystallized samples, the hardness grew from 275.2 HV to the maximum of 397.2 HV after aging for 6 h of AlTi HEA, from 256.5 HV to 387.8 HV after aging for 6 h of AlTiRe HEA, from 250.8 HV to 405.4 HV after aging for 12 h of AlTiRu HEA. This increase in the hardness value can be mainly attributed to the precipitation of $L1_2$ particles. After the peak hardness, there was a slight drop among three HEAs. Then the hardness values kept a moderate fluctuation around 373.4 HV for AlTi HEA till 720 h of aging time, 369.9 HV for AlTiRe HEA and 380.6 HV for AlTiRu HEA, respectively. The higher microhardness of AlTiRu HEA may be related to the precipitation of fine and dispersive $L2_1$ phase. The AlTiRu HEA has lower volume fraction of $L1_2$ precipitates than AlTi and AlTiRe (Fig. 6a) but higher volume fraction of $L2_1$ phase (Fig. 6b). What is more, the grain size of recrystallized sample is 181.1±12.8 μm for AlTi HEA, 172.1±25.9 μm for AlTiRe HEA, 189.1±12.6 μm for AlTiRu HEA, indicating that grain boundary play inevitably small role in the difference of hardness. These results demonstrated that dispersive and fine submicron $L2_1$ particles in AlTiRu HEA (Fig. 1c) had an additional strengthening effect, resulting a slightly higher hardness.

4. Discussion

4.1. Phase stability

Fig. 7a–c present the predicted phase diagrams of the three HEAs, which show the variation of phase mole fraction with temperature. Typical FCC-$L1_2$ dual-phase regions are observed in AlTi and AlTiRe HEAs from 750 ℃ to 1050 ℃, while another NiAl phase emerges in AlTiRu HEA under this temperature range. Notably, the volume fractions of $L1_2$ particles decrease remarkably with temperature rise. At 800 ℃, the mole fraction of $L1_2$ precipitates is 38.27% for AlTi HEA, 38.21% for AlTiRe HEA and 33.68% for AlTiRu HEA. Moreover, the mole fraction of NiAl phase is 2.99% at 800 ℃ for AlTiRu HEA.

Temporal evolution of $L1_2$ volume fraction from experiments during isothermal exposure at temperature of 800 ℃ for the three HEAs is plotted in Fig. 6a. The $L1_2$ volume fraction remained fluctuating slightly and close to the average volume fraction throughout the aging process from 48 h to 720 h among three HEAs. This result demonstrated that the nucleation process had already finished and entered the coarsening regime after 48 h in all the three HEAs, regarded as a stationary coarsening process. The average value of $L1_2$ volume fraction is 40.29% for AlTi HEA, 39.97% for AlTiRe HEA, 34.42% for AlTiRu HEA, respectively, which tentatively approaches the CALPHAD prediction.

Fig. 6b illustrates the change of $L2_1$ volume fraction of the three HEAs with the increase of aging time. For the AlTi HEA and AlTiRe HEA, the value of $L2_1$ volume fraction experienced a sharp rise during the period from 48 h to 192 h. Then it kept a slow fluctuation around 8.7% of AlTi HEA after 192 h, while it reached a plateau at 11.4% of AlTiRe HEA between 360 h and 720 h. Nevertheless, the value of $L2_1$ volume fraction of AlTiRu HEA started to grow dramatically, rising from 7.4% after aging for 48 h to 10.5% after aging for 96 h. Then it fluctuated moderately around 12.4% during the heat treatment process from 192 h to 720 h. Combining the CALPAHD simulation and experimental measurements, we conclude

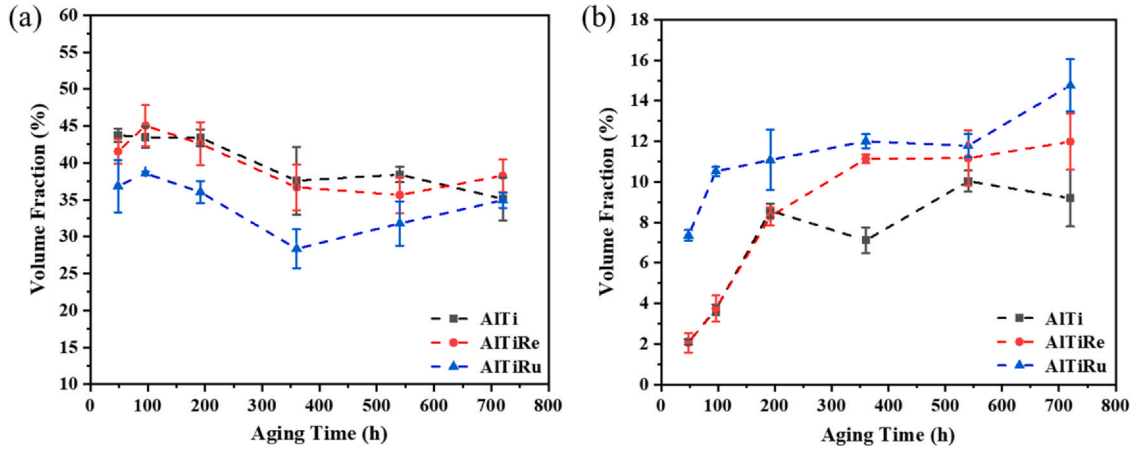

Fig. 6. Temporal evolution of (a) $L1_2$ volume fraction (%) and (b) $L2_1$ volume fraction (%) during isothermal heat-treatment at 800 ℃ of three HEAs.

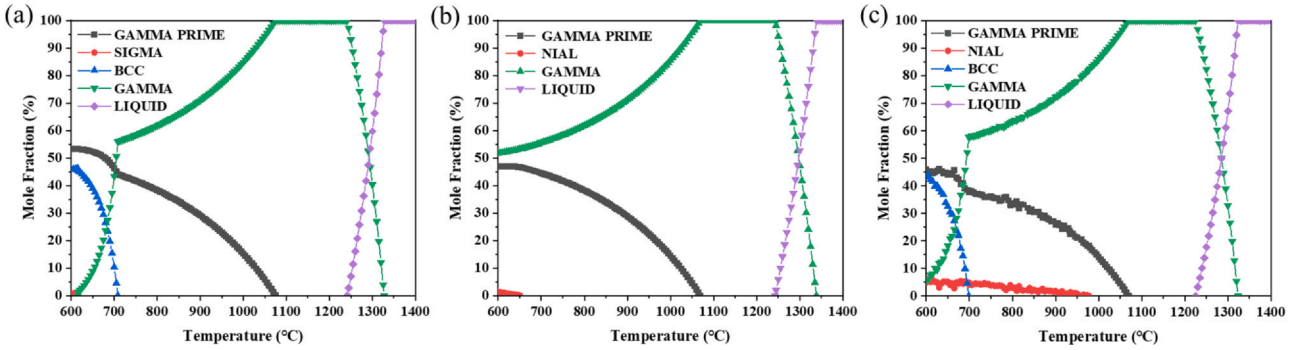

Fig. 7. CALPHAD prediction of three nominal HEAs; (a) $Ni_{29}Co_{27}Fe_{27}Cr_3Al_7Ti_7$ HEA, (b) $Ni_{28}Co_{27}Fe_{27}Cr_3Al_7Ti_7Re_1$ HEA, (c) $Ni_{28}Co_{27}Fe_{27}Cr_3Al_7Ti_7Ru_1$ HEA.

that the AlTi HEA consists of ~40% $L1_2$ phase. The addition of minor Re did not change the volume fraction of $L1_2$ phase, while the minor Ru addition decreased the volume fraction of $L1_2$ phase by ~5%. Both Re and Ru facilitated the formation of $L2_1$ phase to some extent.

The formation of $L2_1$ phase is within understanding, even though it is absent in CALPHAD predicted phase diagram. According to previous reports, a minor Al and Ti alloying addition could produce nanosized $L1_2$ reinforcing phase in FCC-NiCoFeCr HEA matrix, as well as blocky Ni_2AlTi phase with a $L2_1$ Heusler-like structure near the grain boundary [6]. Yang et al. [15]. argued that high Al and Ti supersaturations within the GBs promoted the formation of $L2_1$ phase. Such a $L2_1$-type Heusler phase was also found in other HEAs, such as $(FeCoNiCr)_{100-x-y}Ti_xAl_y$ HEAs [27] and CoCrCuFeNiAlTi HEA [28]. In the present study, Al and Ti elements markedly partitioned to blocky particles in our three HEAs (Fig. 2), and thus reasonably formed the $L2_1$ phase. Moreover, the predicted phase diagrams are based on superalloy database, which may also bring some uncertainties in quantified information.

4.2. Coarsening kinetics of the $L1_2$-type precipitate

The corresponding normalized particle size distributions (PSD) histograms analyzed by commercial ImageJ software are also presented accordingly, as shown in Fig. 8. For a clear comparison, the distribution functions predicted by the LSW theory are plotted here (red curves) [29]. It is evident that the size distribution of the $L1_2$ precipitates in the three HEAs is in reasonable agreement with the prediction by the LSW model, thus indicating that the coarsening of $L1_2$ precipitates is an approximately stationary process [19].

The coarsening kinetics and associated mechanisms of the $L1_2$-type precipitates in the FCC matrix have been extensively studied by various investigators, particularly in case of superalloys [19,30,31,32]. The original model of coarsening for dilute system, the LSW model is based on evaporation of solute atoms from the shrinking particles and its condensation on the growing particles [29,33,34]. According to the LSW theory, the relationship between the $L1_2$ particle diameter and aging time can be written as follows:

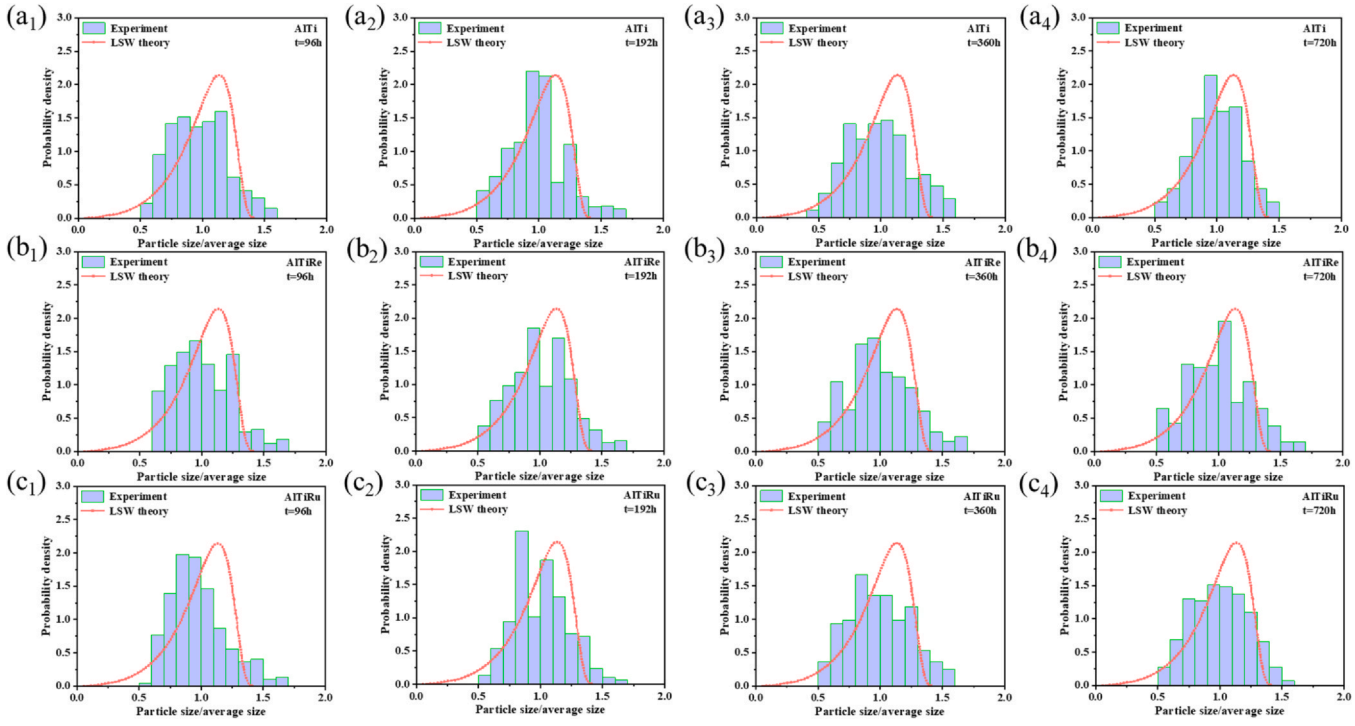

Fig. 8. The particle size distributions of three HEAs aged at 800 ℃ for different time; (a) $Ni_{29}Co_{27}Fe_{27}Cr_3Al_7Ti_7$ HEA, (b) $Ni_{28}Co_{27}Fe_{27}Cr_3Al_7Ti_7Re_1$ HEA, (c) $Ni_{28}Co_{27}Fe_{27}Cr_3Al_7Ti_7Ru_1$ HEA. (For interpretation of the references to colour in this figure, the reader is referred to the web version of this article.)

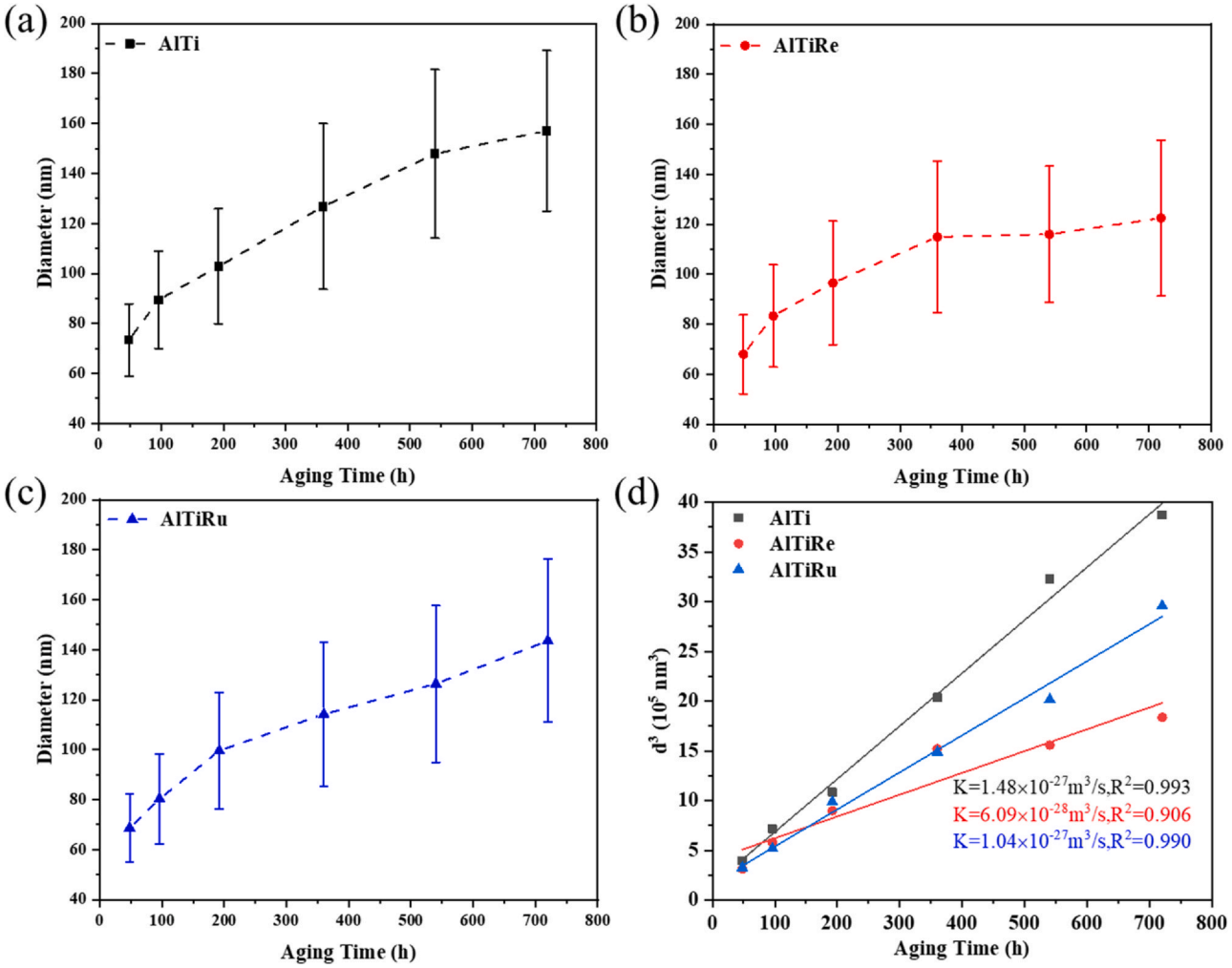

Fig. 9. Precipitation behaviors of three HEAs aged at 800 °C; (a-c) The average diameter evolution of $L1_2$ phase. (b) The LSW relationships using linear regression analysis give slope values corresponding to coarsening rate constants.

$$d^3(t) - d^3(t_0) = k(t - t_0)$$

where $\boldsymbol{d}(\boldsymbol{t})$ represents the average particle size at aging time $\boldsymbol{t}$, $\boldsymbol{d}(\boldsymbol{t_0})$ is the average precipitate size at the onset of coarsening, $\boldsymbol{k}$ is the $L1_2$ particles coarsening rate constant.

Fig. 9a–c shows the average diameter evolution of $L1_2$ particles with aging time of the three HEAs. The increase in aging time led to the ripening of $L1_2$ particles for all the three HEAs, with declining growth rate. The variations of d^3 as a function of t are plotted in Fig. 9d and the coarsening constants at 800 °C for the three HEAs are determined to be 1.48×10^{-27}, 6.09×10^{-28} and $1.04 \times 10^{-27} m^3/s$ by linear fitting to the data set. The coarsening constants of our investigated HEAs and some typical Ni-based superalloys are compared in Table 2. The ripening rate of $L1_2$ precipitate in $Ni_{29}Co_{27}Fe_{27}Cr_3Al_7Ti_7$ HEA is considerably smaller than that in Nimonic 105 [35] and Ni-21.7Co-13.4Al [36]. Moreover, the addition of minor Re and Ru can further increase the coarsening resistance of $L1_2$ precipitates to some degree. It is worthy mentioning that the coarsening rate at 800 °C of the AlTi HEA is slightly faster than some of recently reported HEAs, such as the $Ni_{28}Co_{28}Fe_{21}Cr_{15}Al_4Ti_4$ [13]. It can be expected that the coarsening resistance would be improved further through compositional optimization, such as suitably increasing the content of Cr element.

As Fig. 9d demonstrated, the temporal exponent of the coarsening kinetic is about 3, which means the coarsening kinetic is governed by the volume-diffusion mechanism [12]. Karunaratne et al. [25]. reported that the interdiffusion coefficients of Re and Ru in pure Ni were minimal for the third and second series of transition elements respectively. What is more, Neumeier et al. [17]. published similar diffusing results of Re and Ru in pure Co with experimental data complemented by first-principles calculations. In the present study, minor Re addition significantly retards the coarsening of $L1_2$ precipitates, which can be attributed to the sluggish diffusion of Re in FCC matrix. In addition, it is noteworthy that the effect of Ru on $L1_2$ ripening is more modest compared to Re. On the one hand, the interdiffusion coefficients of Ru in Ni and Co are an order of magnitude larger than that of Re approximately [17,25]. On the other hand, Re mainly partitions to the FCC matrix and $L1_2$ precipitates, which remarkably influences the coarsening process of $L1_2$ precipitates, while Ru principally partitions to $L2_1$ phase according to component analysis (Fig. 2).

5. Conclusion

In this study, the effect of Re and Ru on the phase stability and coarsening behaviors of $L1_2$ phase in the $Ni_{29}Co_{27}Fe_{27}Cr_3Al_7Ti_7$ high entropy alloy was studied using SEM, XRD, and CALPHAD. The following conclusions can be summarized.

(1) High entropy alloy of $Ni_{29}Co_{27}Fe_{27}Cr_3Al_7Ti_7$ exhibits nanometer $L1_2$ phase embedded in the FCC matrix, with presence of micron $L2_1$ precipitates, after prolonged thermal exposure at 800 °C. The

addition of minor Re does not affect the distribution and size of $L2_1$ precipitates, while minor Ru promotes the formation of dispersive and submicron $L2_1$ particles in both GBs region and grain interior. This is because Re partitioned to matrix of AlTiRe HEA, while Ru partitioned to $L2_1$ precipitates in AlTiRu HEA.

(2) The average value of $L1_2$ volume fraction is 40.29% for AlTi HEA, 39.97% for AlTiRe HEA, 34.42% for AlTiRu HEA. After 720 h of isothermal heat treatment, the volume fraction of $L2_1$ phase is 8.7% for AlTi HEA, 11.4% for AlTiRe HEA, 12.4% for AlTiRu HEA, respectively. Both Re and Ru promoted the formation of $L2_1$ phase to some degree.

(3) The $L1_2$ particles remain cubes with round corners for all the three HEAs during ripening process. The coarsening constants of $L1_2$ phase at 800 °C for the three HEAs are determined to be 1.48×10^{-27}, 6.09×10^{-28} and $1.04 \times 10^{-27} m^3/s$. The addition of Re and Ru can retard coarsening of $L1_2$ phase effectively. The sluggish coarsening kinetics is attributed to the slow diffusion of Re and Ru atoms.

(4) The addition of Re and Ru slightly influenced the hardness of $Ni_{29}Co_{27}Fe_{27}Cr_3Al_7Ti_7$ HEA. Particularly, the addition of Ru increased the microhardness slightly, compared to AlTi and AlTiRe HEAs, because it enhanced the volume fraction and decreased the size of $L2_1$ phase.

CRediT authorship contribution statement

Kaiwei Zhang: Formal analysis, Investigation, Resources, Writing - original draft. **Feng He:** Conceptualization, Methodology, Writing - review & editing, Visualization. **Zhongsheng Yang:** Resources, Visualization. **Dingcong Cui:** Resources, Visualization. **Junjie Li:** Supervision, Project administration. **Zenan Yang:** Supervision, Project administration. **Jincheng Wang:** Supervision, Funding acquisition. **Zhijun Wang:** Conceptualization, Methodology, Supervision, Funding acquisition.

Declaration of Competing Interest

The authors declare that they have no known competing financial interests or personal relationships that could have appeared to influence the work reported in this paper.

Acknowledgements

The authors are grateful for the financial support from the National Key Research and Development Program of China (No. 2018YFB1106003), National Natural Science Foundation of China (Nos. 51771149, 52001266, and 51901119), Natural Science Foundation of Shaanxi Province in China (No. 2020JQ-720), and BIAM YiCai Youth Foundation Program (Grant No. KJ53200134).

References

[1] D.B. Miracle, O.N. Senkov, A critical review of high entropy alloys and related concepts, Acta Mater. 122 (2017) 448–511.
[2] T. Yang, Y.L. Zhao, W.P. Li, C.Y. Yu, J.H. Luan, D.Y. Lin, L. Fan, Z.B. Jiao, W.H. Liu, X.J. Liu, J.J. Kai, J.C. Huang, C.T. Liu, Ultrahigh-strength and ductile superlattice alloys with nanoscale disordered interfaces, Science 369 (2020) 427–432.
[3] K. Ming, X. Bi, J. Wang, Realizing strength-ductility combination of coarse-grained $Al_{0.2}Co_{1.5}CrFeNi_{1.5}Ti_{0.3}$ alloy via nano-sized, coherent precipitates, Int. J. Plast. 100 (2018) 177–191.
[4] W.H. Liu, Z.P. Lu, J.Y. He, J.H. Luan, Z.J. Wang, B. Liu, Y. Liu, M.W. Chen, C.T. Liu, Ductile $CoCrFeNiMo_x$ high entropy alloys strengthened by hard intermetallic phases, Acta Mater. 116 (2016) 332–342.
[5] F. He, D. Chen, B. Han, Q. Wu, Z. Wang, S. Wei, D. Wei, J. Wang, C.T. Liu, J. jung Kai, Design of $D0_{22}$ superlattice with superior strengthening effect in high entropy alloys, Acta Mater. 167 (2019) 275–286.
[6] J.Y. He, H. Wang, H.L. Huang, X.D. Xu, M.W. Chen, Y. Wu, X.J. Liu, T.G. Nieh, K. An, Z.P. Lu, A precipitation-hardened high-entropy alloy with outstanding tensile properties, Acta Mater. 102 (2016) 187–196.
[7] Y. Tong, D. Chen, B. Han, J. Wang, R. Feng, T. Yang, C. Zhao, Y.L. Zhao, W. Guo, Y. Shimizu, C.T. Liu, P.K. Liaw, K. Inoue, Y. Nagai, A. Hu, J.J. Kai, Outstanding tensile properties of a precipitation-strengthened $FeCoNiCrTi_{0.2}$ high-entropy alloy at room and cryogenic temperatures, Acta Mater. 165 (2019) 228–240.
[8] T. Yang, Y.L. Zhao, Y. Tong, Z.B. Jiao, J. Wei, J.X. Cai, X.D. Han, D. Chen, A. Hu, J.J. Kai, K. Lu, Y. Liu, C.T. Liu, Multicomponent intermetallic nanoparticles and superb mechanical behaviors of complex alloys, Science 362 (2018) 933–937.
[9] Y.L. Zhao, T. Yang, Y.R. Li, L. Fan, B. Han, Z.B. Jiao, D. Chen, C.T. Liu, J.J. Kai, Superior high-temperature properties and deformation-induced planar faults in a novel $L1_2$-strengthened high-entropy alloy, Acta Mater. 188 (2020) 517–527.
[10] J. Chen, X. Zhou, W. Wang, B. Liu, Y. Lv, W. Yang, D. Xu, Y. Liu, A review on fundamental of high entropy alloys with promising high–temperature properties, J. Alloy. Compd. 760 (2018) 15–30.
[11] Y.Y. Zhao, H.W. Chen, Z.P. Lu, T.G. Nieh, Thermal stability and coarsening of coherent particles in a precipitation-hardened $(NiCoFeCr)_{94}Ti_2Al_4$ high-entropy alloy, Acta Mater. 147 (2018) 184–194.
[12] Y. Zhao, T. Yang, B. Han, J. Luan, D. Chen, W. Kai, C.T. Liu, J. jung Kai, Exceptional nanostructure stability and its origins in the CoCrNi-based precipitation-strengthened medium-entropy alloy, Mater. Res. Lett. 7 (2019) 152–158.
[13] H. Peng, L. Hu, L. Li, W. Zhang, Ripening of $L1_2$ nanoparticles and their effects on mechanical properties of, Mater. Sci. Eng. A 772 (2020) 138803.
[14] F. He, K. Zhang, G. Yeli, Y. Tong, D. Wei, J. Li, Z. Wang, J. Wang, J. jung Kai, Anomalous effect of lattice misfit on the coarsening behavior of multicomponent $L1_2$ phase, Scr. Mater. 183 (2020) 111–116.
[15] T. Yang, Y.L. Zhao, L. Fan, J. Wei, J.H. Luan, W.H. Liu, C. Wang, Z.B. Jiao, J.J. Kai, C.T. Liu, Control of nanoscale precipitation and elimination of intermediate-temperature embrittlement in multicomponent high-entropy alloys, Acta Mater. 189 (2020) 47–59.
[16] F. Pyczak, B. Devrient, F.C. Neuner, H. Mughrabi, The influence of different alloying elements on the development of the γ/γ' microstructure of nickel-base superalloys during high-temperature annealing and deformation, Acta Mater. 53 (2005) 3879–3891.
[17] S. Neumeier, H.U. Rehman, J. Neuner, C.H. Zenk, S. Michel, S. Schuwalow, J. Rogal, R. Drautz, M. Göken, Diffusion of solutes in fcc Cobalt investigated by diffusion couples and first principles kinetic Monte Carlo, Acta Mater. 106 (2016) 304–312.
[18] J. Zhang, L. Liu, T. Huang, J. Chen, K. Cao, X. Liu, J. Zhang, H. Fu, Coarsening kinetics of γ' precipitates in a Re-containing Ni-based single crystal superalloy during long-term aging, J. Mater. Sci. Technol. 62 (2021) 1–10.
[19] P. Pandey, A.K. Sawant, B. Nithin, Z. Peng, S.K. Makineni, B. Gault, K. Chattopadhyay, On the effect of Re addition on microstructural evolution of a CoNi-based superalloy, Acta Mater. 168 (2019) 37–51.
[20] K.E. Yoon, R.D. Noebe, D.N. Seidman, Effects of rhenium addition on the temporal evolution of the nanostructure and chemistry of a model Ni-Cr-Al superalloy. II: analysis of the coarsening behavior, Acta Mater. 55 (2007) 1159–1169.
[21] A.P. Ofori, C.J. Rossouw, C.J. Humphreys, Determining the site occupancy of Ru in the $L1_2$ phase of a Ni-base superalloy using ALCHEMI, Acta Mater. 53 (2005) 97–110.
[22] Z. Peng, I. Povstugar, K. Matuszewski, R. Rettig, R. Singer, A. Kostka, P.P. Choi, D. Raabe, Effects of Ru on elemental partitioning and precipitation of topologically close-packed phases in Ni-based superalloys, Scr. Mater. 101 (2015) 44–47.
[23] L.J. Carroll, Q. Feng, J.F. Mansfield, T.M. Pollock, Elemental partitioning in Ru-containing nickel-base single crystal superalloys, Mater. Sci. Eng. A 457 (2007) 292–299.
[24] D.J. Sauza, P.J. Bocchini, D.C. Dunand, D.N. Seidman, Influence of ruthenium on microstructural evolution in a model Co-Al-W superalloy, Acta Mater. 117 (2016) 135–145.
[25] M.S.A. Karunaratne, R.C. Reed, Interdiffusion of the platinum-group metals in nickel at elevated temperatures, Acta Mater. 51 (2003) 2905–2919.
[26] T. Zheng, X. Hu, F. He, Q. Wu, B. Han, C. Da, J. Li, Z. Wang, J. Wang, J. Kai, Z. Xia, C.T. Liu, Tailoring nanoprecipitates for ultra-strong high-entropy alloys via machine learning and prestrain aging, J. Mater. Sci. Technol. 69 (2020) 156–167.
[27] J.Y. He, H. Wang, Y. Wu, X.J. Liu, H.H. Mao, T.G. Nieh, Z.P. Lu, Precipitation behavior and its effects on tensile properties of FeCoNiCr high-entropy alloys, Intermetallics 79 (2016) 41–52.
[28] D. Choudhuri, T. Alam, T. Borkar, B. Gwalani, A.S. Mantri, S.G. Srinivasan, M.A. Gibson, R. Banerjee, Formation of a Huesler-like $L2_1$ phase in a CoCrCuFeNiAlTi high-entropy alloy, Scr. Mater. 100 (2015) 36–39.
[29] I.M. Lifshitz, V.V. Slyozov, The kinetics of precipitation from supersaturated solid solutions, J. Phys. Chem. Solids 19 (1961) 35–50.
[30] Y. Wu, C. Li, X. Xia, H. Liang, Q. Qi, Y. Liu, Precipitate coarsening and its effects on the hot deformation behavior of the recently developed γ'-strengthened superalloys, J. Mater. Sci. Technol. 67 (2021) 95–104.
[31] S. Jiang, Z. Tian, W. Liu, H. Chen, Z. Yang, Z. Liu, C. Zhang, Y. Weng, Microstructural evolution and hardness of a heat resistant alloy during long term aging at 700 °C, J. Alloy. Compd. 765 (2018) 1267–1274.
[32] Y. Guan, Y. Liu, Z. Ma, H. Li, H. Yu, Precipitation and coarsening behavior of γ' phase in CoNi-base superalloy under different aging treatments, Vacuum 175 (2020) 109247.
[33] Y. Wu, Y. Liu, C. Li, X. Xia, J. Wu, H. Li, Coarsening behavior of γ' precipitates in the $\gamma'+\gamma$ area of a Ni_3Al-based alloy, J. Alloy. Compd. 771 (2019) 526–533.
[34] P. Pandey, S. Kashyap, D. Palanisamy, A. Sharma, K. Chattopadhyay, On the high temperature coarsening kinetics of γ' precipitates in a high strength $Co_{37.6}Ni_{35.4}Al_{9.9}Mo_{4.9}Cr_{5.9}Ta_{2.8}Ti_{3.5}$ fcc-based high entropy alloy, Acta Mater. 177 (2019) 82–95.
[35] P.K. Footner, B.P. Richards, Long - term growth of superalloy γ' particles, J. Mater. Sci. 17 (1982) 2141–2153.
[36] C.K.L. Davies, P. Nash, R.N. Stevens, Precipitation in Ni-Co-Al alloys - part 1 continuous precipitation, J. Mater. Sci. 15 (1980) 1521–1532.